ANALYSIS OF MULTI-TEMPORAL TERRASAR-X IMAGERY OVER A SEMI-ARID REGION IN DARFUR, WESTERN SUDAN

Bernard Spies[1,2], Sarah Brown[1], Alistair Lamb[1], Heiko Balzter[2] and Peter Fisher[2]

1. Astrium GEO-Information Services, Leicester, United Kingdom; bernard.spies@astrium.eads.net
2. University of Leicester, Department of Geography, Leicester, United Kingdom

ABSTRACT

The purpose of this study was to assess the relationship between radar backscatter values (σ^o) and NDVI values over a semi-arid region in Darfur. Three HH-polarised, 26° incidence angle TerraSAR-X imagery from different seasonal dates were compared to Landsat and RapidEye images, available closest to the same dates. Samples of six land cover classes were selected from the SAR and optical imagery and distribution graphs were compared. The land cover classes for Urban, Vegetation and Agriculture showed a good relationship between σ^o and NDVI. The relationship between σ^o and NDVI for land cover classes Bare, Perennial river and River bank was a lot weaker. Probability distribution graphs were compared for the six chosen land cover classes. It was shown that multi-temporal TerraSAR-X imagery (HH-polarised, 26° incidence angle) can separate more classes than single date images, but not all six classes. It is planned to investigate the contribution of multi-polarimetric and multi-frequency SAR to improve the separation of classes for the same area in further research.

INTRODUCTION

The tropical and sub-tropical parts of the world are often covered by cloud. Since SAR sensors are generally not affected by cloud cover, the use of SAR to monitor seasonal changes and for longer time-series of land cover change over these areas is proposed. There are many factors and parameters influencing the interpretation of SAR backscatter values, which include the frequency, polarisation, incidence angle and spatial resolution (1). These different parameters used in SAR systems all have different scattering mechanisms of surface scattering and volume scattering as they interact with the geometric characteristics and water content (dielectric constant) of soils/vegetation and other land cover types (2). The understanding of the parameters involved is therefore paramount for the interpretation of the backscatter recorded by the SAR sensor.

Synthetic aperture radar (SAR) is frequently used to assist in emergency response situations (3). Currently SAR is mostly used to monitor flooding, forest storm damage and landslide mapping. The all-weather capability of SAR makes it an appealing candidate to use when timely data is crucial, such as for emergency response situations (4). The use of SAR to map land cover change is proposed to enable mapping updates of areas where information is required for emergency response situations. This will allow mapping of areas of interest under any atmospheric conditions, be it cloud cover or low illumination conditions at high latitudes. The capacity of satellites to repeatedly and regularly revisit the same area enables multi-temporal analysis to be carried out (5).

The main objective of this study is to assess the relationship between radar backscattering coefficient (σ^o) values from TerraSAR-X images and normalised difference vegetation index (NDVI) values from medium resolution optical imagery. TerraSAR-X images and NDVI values was compared in (6) to monitor the harvest season of sugarcane. High correlation between TerraSAR-X and SPOT data was found and the phenological trend and harvest times were clearly observed in the radar signal for sugarcane. It was concluded that the precipitation influences the radar signal significantly especially at low and medium incidence angles. Another conclusion was that for crops with significant biomass, X-band is not the optimal frequency. However, in this study X-band was

still investigated as the study area was a semi-arid landscape, without too dense vegetation. In a recent review article on deriving above ground biomass (AGB) for semi-arid regions, several techniques to derive AGB using optical and SAR data were listed (3). Most of the optical approaches used NDVI or similar measure to derive AGB. To derive AGB from SAR, L-band and C-band were used most often. However, the relationship between X-band and NDVI values will give an indication of how X-band SAR could be used to derive biomass, and for general land cover classification of semi-arid regions. In this current study several land cover classes (Urban, Vegetation, Agriculture, Bare, Perennial river and River bank areas) were compared to assess the relationship between X-band σ^o values and NDVI values. Secondly, the different distributions of SAR backscatter values for each land cover class were compared, to assess whether the chosen land cover classes can be separated satisfactorily with the available multi-temporal TerraSAR-X data.

METHODS

The study area was located in Darfur, in the Western part of Sudan. The study area was monitored to assess changing land cover types surrounding a town with many internally displaced persons (IDPs). The data were acquired for a previously conducted Services and Applications for Emergency Response (SAFER) project, part of Global Monitoring of Environment and Security (GMES) in 2010. Three TerraSAR-X images were available for for the study area; in January, April and August 2010. All three available TerraSAR-X images were HH-polarised, with incidence angle 26°. Therefore, the only changing variable in the σ^o values was the temporal difference of the changing land cover, i.e. either seasonal or man-made changes to the land cover. Six land cover classes were chosen to investigate, namely Urban, Vegetation, Agriculture, Bare, Perennial river and River bank areas. Being able to classify these land cover types will assist in the understanding of the environmental changes occuring where there are large movements of population and could be useful for aid-organisations during emergency response situations.

The study area forms part of the Sudanese savannas, just south of the Sahel. The Sahel is a transition zone between the Sahara desert and the Sudanese savannas. In the GLC2000 map, the study area was classified as a combination of Croplands (>50%), Croplands with open woody vegetation and Open Grassland with sparse shrubs at 1km scale using data from the year 2000 (7).

Pre-processing of SAR and optical data

The TerraSAR-X images were compared to NDVI values from optical satellite images. Two Landsat images coincided with the January and April TerraSAR-X images. One RapidEye image was available close to the August TerraSAR-X image. The pre-processing steps for the optical and SAR imagery are shown in Figure 1.

To enable scene-to-scene comparison, the optical images had to be converted from radiance (L_λ) to top-of-atmosphere reflectance (ρ_λ) (8). Similarly, the TerraSAR-X images had to be calibrated from digital numbers (DN) to radar backscattering coefficients, σ^o (9). The calibration was done using NEST software, where a simplified approach is implemented, excluding the Noise equivalent Beta Naught term (10).

Sampling methodology

Representative sample areas were chosen from the multi-date TerraSAR-X imagery and corresponding optical imagery. Samples were chosen to fall within the Landsat 7 data range, outside the scan line corrector missing data. A 30m x 30m grid was calculated by a chessboard segmentation algorithm. This coincided to the 30m x 30m spatial resolution of the Landsat images. The arithmetic mean value of each grid area was calculated to reduce the effect of speckle from the SAR images, combing a hundred 3m x 3m pixels into one 30m grid cell. The RapidEye image resolution was reduced from 7.5m to 30m.

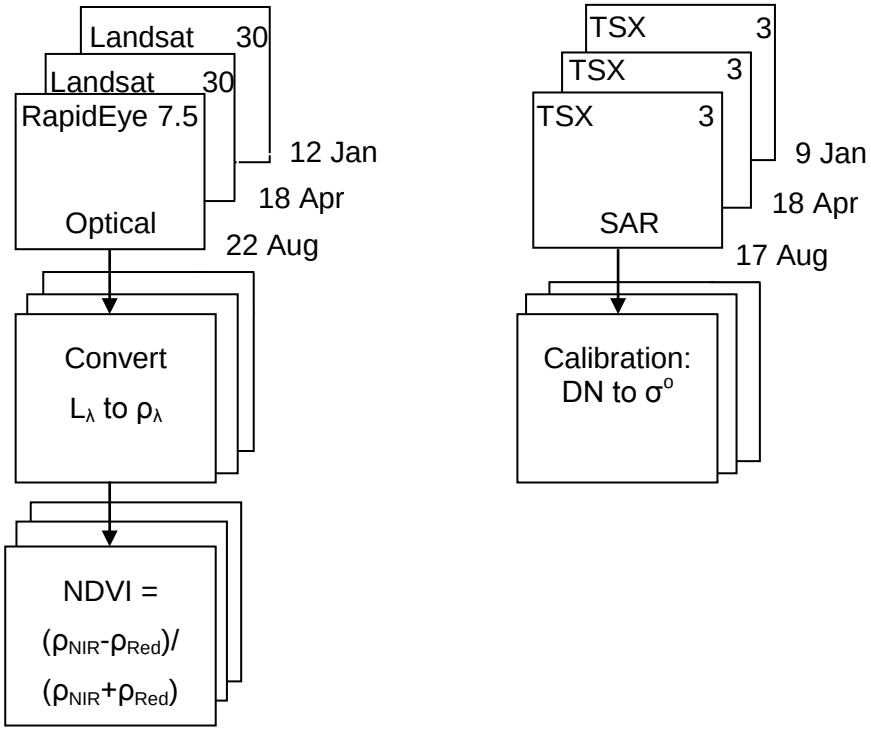

Figure 1: Pre-processing steps for optical imagery to calculate reflectance for each band (ρ_λ) and NDVI values and to calibrate SAR imagery from DN to σ^o. The dates and imagery available are shown in the diagram. The spatial resolution is given in top right-hand side of each image representation.

Thirty-six sample areas were selected for each land cover class. This allowed the calculation of mean and standard deviation values to estimate probability distribution functions, assuming a gaussian distribution of the σ^o values. The mean and standard deviation values were calculated from the NDVI values for the three optical images. This was a simplified approach to compare the general distribution of the σ^o values of the each land cover class, and the possible non-gaussian distribution of each land cover class such as in (11), was excluded from this research.

RESULTS

Comparison of NDVI and σ^o

The σ^o values were compared to the NDVI values by plotting both on the same axis for each land cover class. The TerraSAR-X σ^o values were compared to the NDVI values for the closest matching dates during January, April and August 2010. These comparison graphs are shown in Figure 2 for each of the six land cover classes. The σ^o values for Urban, Vegetation and Agriculture classes followed the same trend as the NDVI values. The σ^o values for Bare, Perennial River and River bank had a much weaker relationship to the NDVI values. It was noted that most of the Bare areas are in mountainous terrain, which would affect the local incidence angle of the radar signal, and therefore the measured σ^o values. In general SAR has low backscatter values for open water. The changing NDVI values for the Perennial river and River bank areas were probably related to vegetation growth in the water. Unfortunately no ground truth data or high resolution satellite imagery for each of the three dates is available to validate the exact ground cover for these classes at each date.

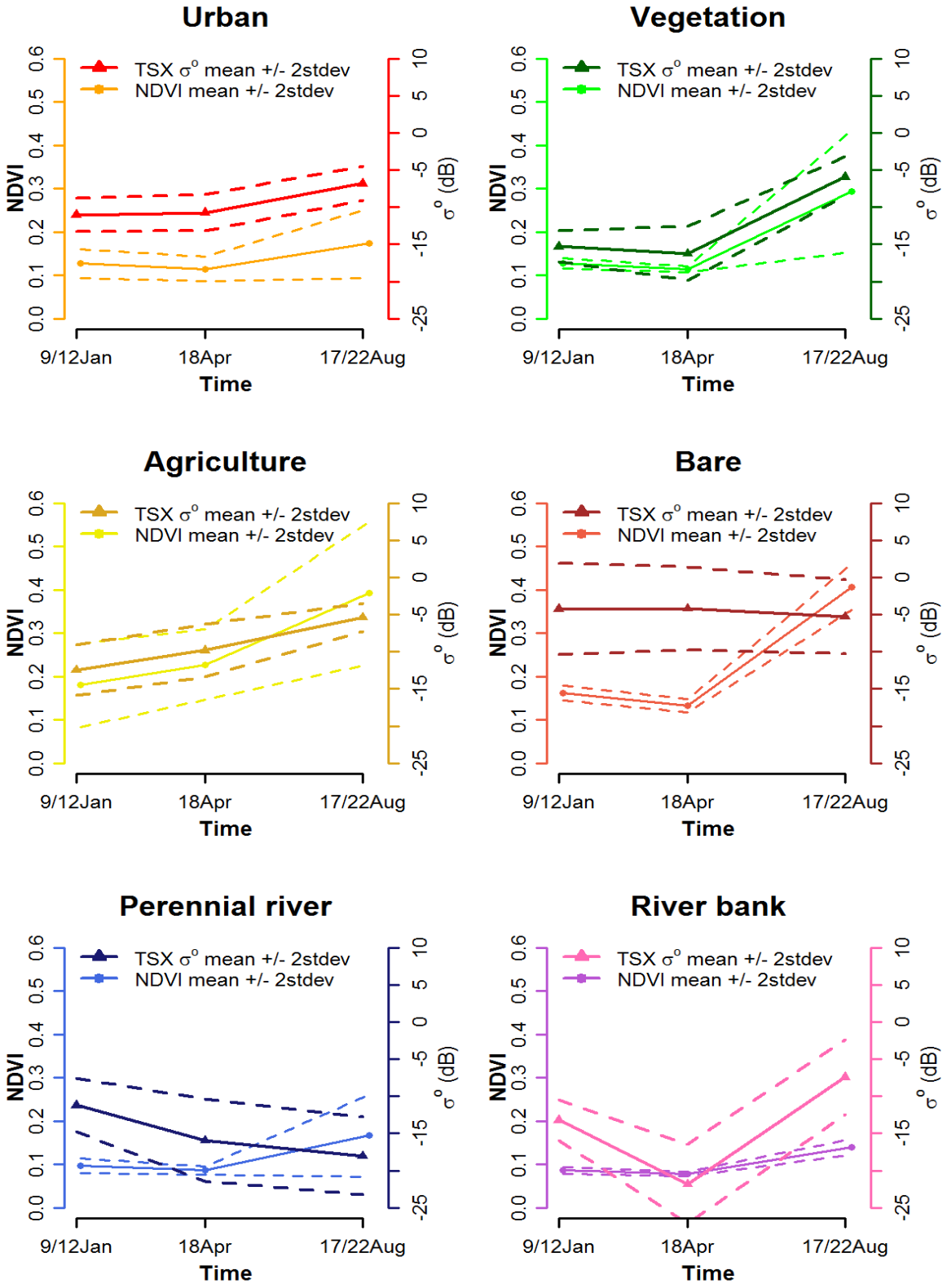

Figure 2: Comparison of σ° values with NDVI values for six land cover classes. The solid lines show the mean values, whereas the dashed lines show two times the standard deviation values.

Class separation using σ° values

The radar backscatter coefficient values were compared for each of the six classes for the three available dates, as shown in Figure 3.

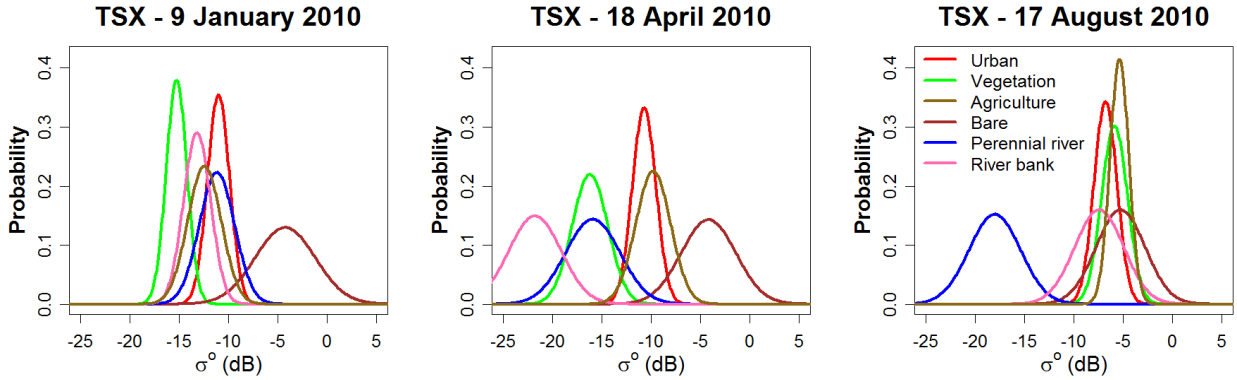

Figure 3: Comparison of the distribution of radar backscatter of six land cover classes for three TerraSAR-X images for 9 January, 18 April and 17 August 2010 from selected sample areas.

From single date TerraSAR-X images, it was possible to separate some land cover classes; e.g. Perennial river class in the August image is well separated from all the other classes. By combining the multi-temporal TerraSAR-X images it became possible to separate more classes. For example: Bare and River bank classes, which overlaps in the August image, can be separated by combining the April and August images as the two backscatter distributions are parted in the April image. The Bare class can also be separated from the other classes from the January image. However, Urban and Agriculture classes remain inseparable with current multi-temporal X-band HH-polarised data, as their distributions overlap for each of the three available dates. There is also a significant overlap in the tails of most of the class distributions.

CONCLUSIONS

The σ° values showed similar trends to the NDVI values for Urban, Vegetation and Agriculture for the dates examined. This is comparable to what was found in (6), for sugarcane plantations. The exact relationship between X-band SAR backscatter values and above ground biomass (AGB) for semi-arid regions is an area of further research. As was pointed out in (5) previous studies mostly related L- and C-band SAR to AGB. For the Bare, Perennial river and River bank classes, the σ° values were not as well correlated to the NDVI values. High-resolution imagery at each date would assist to explain this. All six classes could not be separated using multi-temporal (January, April and August) HH-polarised, 26° TerraSAR-X imagery. However, it was shown that X-band radar is sensitive to changes in vegetation in these semi-arid regions. This sensitivity could be valuable in the mapping of these land cover classes if they could be successfully separated.

Possible sources of error may be the selection of the bare samples. The bare areas had high σ° values for all three images. However, the NDVI values showed a definite rise in the August image. This could be due to the specific incidence angle resulting in high backscatter values from mountainous terrain. Investigation of the specific slope of the terrain on these results, using a digital elevation model, still needs to be carried out. Other sources of error may be the filtering algorithm applied; which was an arithmetic mean using chessboard segmentation on the SAR data, and the simplification of assuming a gaussian distribution of the SAR backscatter signal. By taking more samples the specific distribution of the backscatter of each land cover class may be determined.

The use of multi-polarimetric and multi-frequency SAR (L- and C-band) (12,13) to improve class separation will be studied further. The use of semi-empirical and theoretical scattering models to

derive biophysical parameters from SAR backscatter values (5), as an intermediate step to land cover classification will be evaluated in further research.

ACKNOWLEDGEMENTS

GIONET is funded by the European Commission, Marie Curie Programme, Initial Training Networks, Grant Agreement number PITN-GA-2010-264509

REFERENCES

1 Lewis A J, F M Henderson & D W Holcomb, 1998. Radar Fundamentals: The Geoscience Perspective. In: Principles and Applications of Imaging Radar, edited by F M Henderson & A J Lewis (John Wiley & Sons) 131-181

2 Ulaby F T, R K Moore & A. K. Fung, 1982. Microwave Remote Sensing: Active and Passive Volume II: Radar Remote Sensing and Surface Scattering and Emission Theory (Artech House)

3 Voigt S, T Kemper, T Riedlinger, R Kiefl, K Scholte & H Mehl, 2007. Satellite Image Analysis for Disaster and Crisis-Management Support. IEEE Transactions on GeoScience and Remote Sensing, 45:6: 1520-1528

4 Wiesmann A, U Wegmüller, M Honikel, T Strozzi & C L Werner, 2001. Potential and methodology of satellite based SAR for hazard mapping. In: *IEEE Geoscience and Remote Sensing Symposium (IGARSS)*, (IGARSS Sydney), 3-5

5 Eisfelder C, C Kuenzer & S Dech, 2012. Derivation of biomass information for semi-arid areas using remote-sensing data. International Journal of Remote Sensing*, 33:9: 2937-2084*

6 Baghdadi N, Cresson R, Todoroff P & S Moinet, 2010. Multitemporal Observations of Sugarcane by TerraSAR-X Images. Sensors, 10:10: 8899-8919

7 Mayaux P, E Bartholome, S Fritz & A Belward, 2004. A new land-cover map of Africa for the year 2000. Journal of Biogeography, 31: 861-877

8 Chander G, B L Markham & D L Helder, 2009. Summary of current radiometric calibration coefficients for Landsat MSS, TM, ETM+, and EO-1 ALI sensors. Remote Sensing of Environment, 113:5: 893-903

9 Freeman A, 1992. SAR calibration: an overview. IEEE Transactions on Geoscience and Remote Sensing, 30:6: 1107-1121

10 ESA, 2012. "NEST: Next ESA SAR Toolbox. http://nest.array.ca/web/nest (last date accesses: 16 May 2012)

11 Lin Y, K Sarabandi, 1999. A Monte Carlo Coherent Scattering Model For Forest Canopies Using Fractal-Generated Trees. IEEE Transactions on Geoscience and Remote Sensing, 37:1: 440-451

12 Dobson M C, L E Pierce & F T Ulaby, 1997. The Role of Frequency and Polarization in Terrain Classification Using SAR Data, *In: IEEE International Geoscience and Remote Sensing Symposium (IGARSS),* (IGARSS Singapore), 3-5

13 Englhart S, V Keuck & F Siegert, 2012. Modeling Aboveground Biomass in Tropical Forests Using Multi-Frequency SAR Data — A Comparison of Methods. IEEE Journal of Selected Topics in Applied Earth Observations and Remote Sensing, 5:1: 298-306